Potato Res. (2026) 69:172
https://doi.org/10.1007/s11540-026-10124-w

Structural Diversity of Steroidal Glycoalkaloids in Potato (*Solanum tuberosum*) Leaves Revealed by Untargeted UHPLC–QTOF Metabolomics

Gilles Rousseau[1] · **Boris Krings**[1] · **Yordan Muhovski**[2]

Received: 12 May 2026 / Accepted: 2 August 2026

Abstract
Steroidal glycoalkaloids (SGAs) are nitrogenous defence metabolites characteristic of *Solanum* species. Although the major potato SGAs α-solanine and α-chaconine are well known, the full structural scope of glycoalkaloids in vegetative tissues remains largely uncharacterized. Here, we applied untargeted ultra-high-performance liquid chromatography–quadrupole time-of-flight mass spectrometry (UHPLC-QTOF-MS) to profile SGA diversity in the leaves of three cultivars (Lady Rosetta, Charlotte, and Bintje). High-resolution MS/MS data enabled annotation of over 30 tri-glycosylated alkaloids differing in both the steroidal backbone and glycosylation topology. Three compounds, α-solanine, α-chaconine, and α-solamargine, were verified with authentic standards (Metabolomics Standards Initiative (MSI) level 1). Besides classical solanidine-based SGAs, multiple metabolites were consistent with solasodine- and solaverol-type aglycones (MSI level 2–3), revealing unrecognized biosynthetic branches. SGA composition varied strongly among cultivars: Lady Rosetta exhibited the broadest chemical repertoire and the highest abundance of oxygenated SGAs, whereas Bintje displayed a restricted solanidine-dominant profile. Several low-abundance SGAs bearing partially unsaturated or over-oxidized aglycones (*m/z* 396, 412 and 428) were reproducibly detected and likely represent genuine metabolites, hinting at additional, low-flux biosynthetic routes. This comprehensive profile extends the structural landscape of potato SGAs and underscores the capacity of untargeted UHPLC–QTOF metabolomics to resolve complex steroidal metabolite networks. The observed cultivar-specific signatures suggest differential regulation of late-stage oxidation and glycosylation steps, potentially contributing to varietal variation in chemical defence.

Keywords Cultivar variation · Glycosylation diversity · *Solanum tuberosum* · Specialized metabolism · Steroidal glycoalkaloids · UHPLC-QTOF · Untargeted metabolomics

Extended author information available on the last page of the article

Published online: 26 August 2026

Introduction

Steroidal glycoalkaloids (SGAs) constitute a major class of nitrogen-containing specialized metabolites in the genus *Solanum*, where they play a central role in plant defence against herbivores and microbial pathogens (Calf et al. 2018; Martin et al. 2020; Nielsen et al. 2020; Delbrouck et al. 2023). In potato (*Solanum tuberosum* L.), these compounds are predominantly accumulated in aerial tissues and are rapidly mobilized upon biotic stress, contributing to the chemical component of innate immunity (Jared et al. 2016; Calf et al. 2018). However, they are also of toxicological relevance for humans and animals, as excessive consumption can lead to adverse health effects, which has driven sustained interest in their detection, characterization, and quantitative profiling (Golan et al. 2005; Martin et al. 2020; EFSA Panel on Contaminants in the Food Chain (CONTAM) et al. 2020; Delbrouck et al. 2023).

Historically, investigations of potato steroidal glycoalkaloids have focused primarily on the two major metabolites α-solanine and α-chaconine, both derived from the solanidine aglycone. However, recent high-resolution mass spectrometry studies suggest that the steroidal glycoalkaloid metabolome of *Solanum* species is considerably more diverse, encompassing multiple aglycone scaffolds, distinct oxidation states, and variable glycosylation architectures (Friedman et al. 1997; Sonawane et al. 2018; Rodríguez-Pérez et al. 2018; Lelario et al. 2019; Martin et al. 2020; Delbrouck et al. 2023). In particular, the presence of alternative aglycones such as solasodine and solaverol derivatives suggests the existence of parallel or branching biosynthetic routes that remain insufficiently documented in potato (Sonawane et al. 2018; Delbrouck et al. 2023).

The composition and abundance of SGAs are known to vary markedly among potato cultivars and tissues, and these differences have been proposed to contribute to cultivar-specific interactions with biotic stress, although direct functional relationships remain incompletely established (Jared et al. 2016; Calf et al. 2018, 2019; Barre et al. 2019; Scaglione et al. 2021; Middendorf et al. 2022). While tuber glycoalkaloid profiles have been extensively studied due to their food safety implications (Massana-Codina et al. 2020), comparatively little attention has been given to leaf tissues, despite their critical role as primary interfaces with pests and pathogens. Moreover, most existing studies rely on targeted analytical approaches that inherently limit the detection of structurally unexpected or low-abundance SGAs.

Untargeted metabolomics based on ultra-high-performance liquid chromatography coupled to Quadrupole Time-Of-Flight mass spectrometry (UHPLC-QTOF) offers a powerful strategy to overcome these limitations. By combining chromatographic separation and accurate mass measurements with a Data-Dependent Acquisition (DDA) strategy, this approach enables discrimination of isomeric species and reconstruction of biosynthetic series based on shared structural features—capabilities particularly well suited to investigating the chemical diversity of SGAs, including variations in aglycone structure and glycosylation patterns (Lelario et al. 2019; Delbrouck et al. 2023).

In the present study, an untargeted UHPLC–QTOF mass spectrometry approach was applied to comparatively profile SGAs in leaf tissues of three

contrasting *S. tuberosum* cultivars: Lady Rosetta, Charlotte, and Bintje. The objectives were (i) to characterize structural and semi-quantitative diversity of these compounds in potato leaves, (ii) to identify major and low-abundance SGA biosynthetic series based on aglycone precursors and glycosylation motifs, and (iii) to assess cultivar-dependent differences in their composition. By providing a detailed comparative overview of leaf glycoalkaloid species profiles, this work aims to refine current models of their biosynthetic pathways in potato.

Materials and Methods

Plant Material and Growth Conditions

Plants of *Solanum tuberosum* L. cultivars Lady Rosetta, Charlotte, and Bintje were propagated from stem cuttings and grown hydroponically in full strength Hoagland solution (Hoagland and Arnon, 1950) under controlled phytotron conditions at the Walloon Agricultural Research Centre (CRA-W, Gembloux, Belgium). Environmental parameters were maintained constant throughout the experiment: temperature 21 °C/18 °C (day/night), relative humidity 65%, and a photoperiod of 16-h light/8-h dark. Leaf samples were collected from 5-week-old plants. The 3rd and 4th fully expanded leaves from the top were harvested 5 weeks after planting, immediately frozen in liquid nitrogen, ground to a fine powder, and stored at −80 °C until analysis. For each cultivar, three independent biological replicates were collected, each consisting of pooled leaf material from five individual plants.

Chemicals and Analytical Standards

Methanol (LC–MS grade) and formic acid (≥99%) were obtained from commercial suppliers and used without further purification. Ultrapure water (18.2 MΩ·cm resistivity) was produced using a Milli-Q purification system.

Analytical standards of α-solanine (CAS 20562-02−1), α-chaconine (CAS 20562-03−2), and α-solamargine (CAS 20311-51−7) were purchased from Sigma-Aldrich and Merck/PhytoLab. These standards were used to confirm retention times and fragmentation patterns, enabling unambiguous compound identification and assignment at MSI level 1 in sample extracts.

For other SGAs, structural annotations relied on accurate mass, isotope pattern, retention behaviour and diagnostic MS/MS fragmentation, and should therefore be considered putative (MSI level 2 or 3). Due to the absence of compound-specific response factors and internal standards, relative intensity signal comparisons should be interpreted as semi-quantitative estimates.

Sample Preparation and Extraction

Frozen leaf tissue (100 mg fresh weight) was used for metabolite extraction. Metabolites were extracted with 1 mL of a water/methanol solution (80:20, v/v) containing

0.1% (v/v) formic acid. Samples were macerated for 60 min at room temperature, followed by agitation for 20 min and centrifugation at 4800 × g for 7 min at 4 °C.

The resulting supernatants were collected and directly analyzed without hydrolysis in order to preserve intact glycosylated steroidal glycoalkaloids. Each biological replicate was injected in duplicate for UHPLC–MS analysis.

UHPLC–QTOF Mass Spectrometry Analysis

Chromatographic separation was performed using a Nexera X2™ UHPLC system (Shimadzu, USA) equipped with a Waters Acquity HSS T3 column (2.1 × 100 mm, particle size 1.8 µm). The column temperature was maintained at 40 °C and the autosampler temperature at 15 °C. The injection volume was 5 µL.

The mobile phase consisted of (A) water/methanol (95:5, v/v) containing 0.1% formic acid and (B) methanol containing 0.1% formic acid. The flow rate was set to 300 µL min^{-1}. The linear gradient programme was as follows: 0–5 min, 2% B; 5–20 min, 2–98% B; 20–25 min, 98% B; 25–26 min, 98–2% B; 26–35 min, 2% B for column re-equilibration.

Mass spectrometric detection was carried out on an X500R quadrupole time-of-flight mass spectrometer (AB Sciex, Singapore) equipped with an electrospray ionization (ESI) source operated in positive ion mode. Data were acquired over an m/z range of 100–1000 using Data-Dependent Acquisition (DDA). Survey scans were followed by MS/MS experiments using stepped collision energies centred at 35 V. To guarantee mass accuracy, calibration is performed between each group of 5 injections.

To improve structural elucidation, selected samples were reanalyzed using increased declustering potentials and collision energies (up to 60 and 90 V, respectively) to obtain enhanced fragmentation spectra. Internal mass calibration was performed every five injections to ensure high mass accuracy.

Data Processing and Metabolite Annotation

Raw UHPLC–QTOF data were processed using Sciex OS software and further analyzed using XCMS Online for peak detection, alignment, and pairwise comparison. Feature selection was based on statistical filtering using p-values and fold-change thresholds to identify metabolites contributing most strongly to inter-cultivar differences.

Metabolite annotation was performed using accurate mass measurements, isotope patterns, retention behaviour, and MS/MS fragmentation data. Putative identifications were supported by comparison with reference databases, including PlantCyc (S. tuberosum v7.0.0), PubChem, and ChemSpider. Structural assignment of SGAs relied primarily on diagnostic fragment ions corresponding to aglycone cores and characteristic neutral losses associated with glycosyl moieties. Only features exhibiting a mass error ≤ 1 ppm and sufficient signal intensity were retained for structural interpretation.

Metabolite annotation confidence was evaluated according to the Metabolomics Standards Initiative (MSI). Compounds confirmed with analytical standards (α-solanine, α-chaconine, α-solamargine) were assigned to MSI level 1. All other SGAs were considered putatively annotated (level 2 or 3).

Raw and processed metabolomics data associated with this study will be made publicly available via XCMS Online upon publication (Supplementary Fig. S6-S8).

Statistical Analysis

Comparative metabolite profiling was conducted using pairwise statistical analysis implemented in XCMS Online. Relative abundances of SGAs and their corresponding aglycone precursors were calculated from extracted ion chromatograms. Differences between cultivars were assessed based on relative signal intensities, and results are reported as relative signal contribution (%) (semi-quantitative data) within each cultivar rather than absolute concentrations.

Relative abundances were estimated from extracted ion chromatograms and should be interpreted as semi-quantitative, as no internal standard or compound-specific response factor correction was applied.

Results and Discussion

Global Overview of SGA Diversity in Potato Leaves

Untargeted UHPLC–QTOF metabolomic profiling revealed steroidal glycoalkaloids (SGAs) as one of the predominant specialized metabolite classes in potato leaf extracts from the three investigated cultivars. High-resolution MS and MS/MS (Supplementary Figs. S1–S3) analyses enabled the detection of more than 30 tri-glycosylated alkaloids differing in both steroidal aglycone structure and glycosylation topology. Accurate mass measurements (mass error ≤ 1 ppm), reproducible retention times, and characteristic fragmentation patterns allowed reliable discrimination of structurally related compounds and reconstruction of coherent SGA biosynthetic series.

The detected SGAs were mainly organized into homologous metabolite groups sharing common aglycone-related fragment ions but differing in oxidation state and carbohydrate composition. Several compounds corresponded to the well-characterized potato glycoalkaloids α-chaconine and α-solanine, whereas numerous additional metabolites displayed fragmentation patterns consistent with alternative aglycone scaffolds and/or distinct trisaccharide organizations. This highlights a substantially broader structural diversity of potato leaf SGAs than generally represented by targeted analyses restricted to the major solanidine-derived compounds.

Marked cultivar-dependent differences were observed in both the qualitative composition and relative abundance of SGAs (Figs. 4, 5, 6). Lady Rosetta exhibited the highest structural diversity and accumulated numerous oxygenated and low-abundance SGAs, whereas Bintje displayed a comparatively restricted profile

dominated by a limited number of highly abundant compounds. Charlotte showed an intermediate composition between these two cultivars. These metabolic signatures were consistently reproduced across biological replicates, supporting the robustness of the observed cultivar-specific patterns.

Overall, the detected metabolites could be grouped into distinct SGA families according to their aglycone precursor and glycosylation architecture, revealing extensive diversification of steroidal alkaloid metabolism in potato leaves.

Structural Classification of Major SGA Families

Aglycone Diversity and Oxidation Series

Accurate mass measurements and MS/MS fragmentation analyses enabled the classification of the major SGAs detected in potato leaves into four principal aglycone families (Figs. 1, 2, 3, 4): solanidine (C27H43NO, m/z 398), solasodine (C27H43NO2, m/z 414), solaverol A (C27H43NO3, m/z 430), and solaverol B (C27H43NO4, m/z 446). These aglycones form a coherent homologous series differing by successive oxygen additions, suggesting progressive oxidation reactions during the late stages of SGA biosynthesis.

Solanidine-derived SGAs corresponded to the classical potato glycoalkaloids α-chaconine and α-solanine, which were detected in all cultivars and represented the dominant SGA class in Bintje and Charlotte. In contrast, SGAs associated with more oxygenated aglycones displayed a markedly uneven distribution among cultivars. Solasodine-derived compounds accumulated predominantly in Lady Rosetta, where they represented approximately 65% of relative LC–MS signal contribution of total SGAs (Fig. 7), but remained minor constituents in Charlotte (~2.3%) and Bintje (~1.2%). More highly oxygenated solaverol-derived SGAs were detected almost exclusively in Lady Rosetta, indicating enhanced diversification of oxidative transformations in this cultivar.

The occurrence of solasodine- and solaverol-type SGAs expands the currently recognized structural diversity of potato leaf glycoalkaloids. Similar oxygenated steroidal alkaloids have previously been described in other *Solanum* species, including the solaverines (Yamashita et al. 1990; Lelario et al. 2019; Razgonova et al. 2023), supporting the plausibility of related biosynthetic pathways in potato. Together, these observations suggest that potato SGA metabolism involves a broader oxidation continuum than generally represented by the classical α-solanine/α-chaconine model.

Glycosylation Topology and Structural Discrimination

In addition to aglycone diversity, substantial structural variation was associated with glycosylation topology. MS/MS fragmentation spectra revealed that most detected SGAs were predominantly tri-glycosylated and composed of combinations of hexose and deoxyhexose residues. Two principal trisaccharide organizations were consistently observed: branched Y-shaped structures and linear trisaccharides. Among

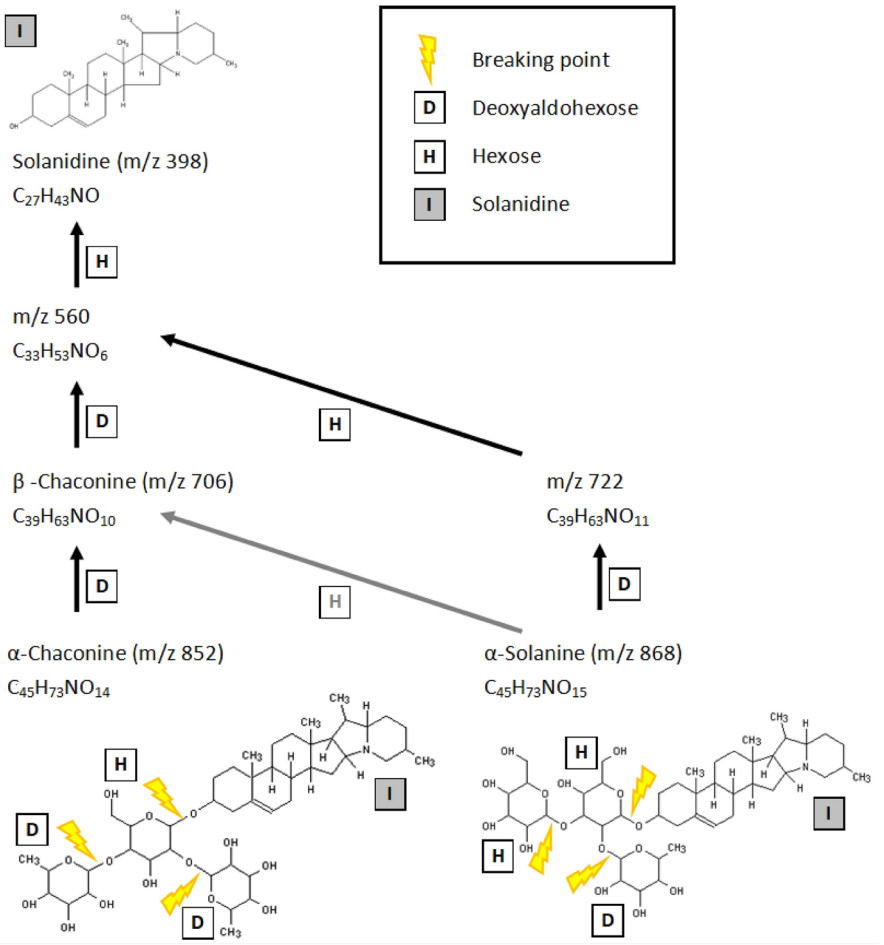

Fig. 1 Fragmentation patterns of α-solanine (*m/z* 868; compound B4 (Table 3)) and α-chaconine (*m/z* 852; compound A). Solanidine (I) is the common alkaloid precursor. Glycosylation with one hexose (D-glucose) and two deoxyhexose (L-rhamnose) residues yields α-chaconine, whereas glycosylation with two hexose residues (D-galactose and D-glucose) and one deoxyhexose residue (L-rhamnose) yields α-solanine. These SGAs correspond to compounds A, B4, and B5 in Table 3

Y-shaped trisaccharides, only those containing two hexose units attached to the aglycone core displayed characteristic dual fragmentation pathways, corresponding to the alternative initial loss of either a hexose or a deoxyhexose residue. In contrast, Y-shaped trisaccharides containing a single hexose unit did not exhibit this diagnostic spectral pattern. Linear trisaccharides generally showed sequential monosaccharide losses during MS/MS fragmentation and tended to elute earlier during chromatographic separation, consistent with their higher polarity and weaker interaction with the stationary phase. Together, these complementary spectral and chromatographic features enabled reliable structural discrimination between isomeric forms (Figs. 1, 2, 3 and Table 1).

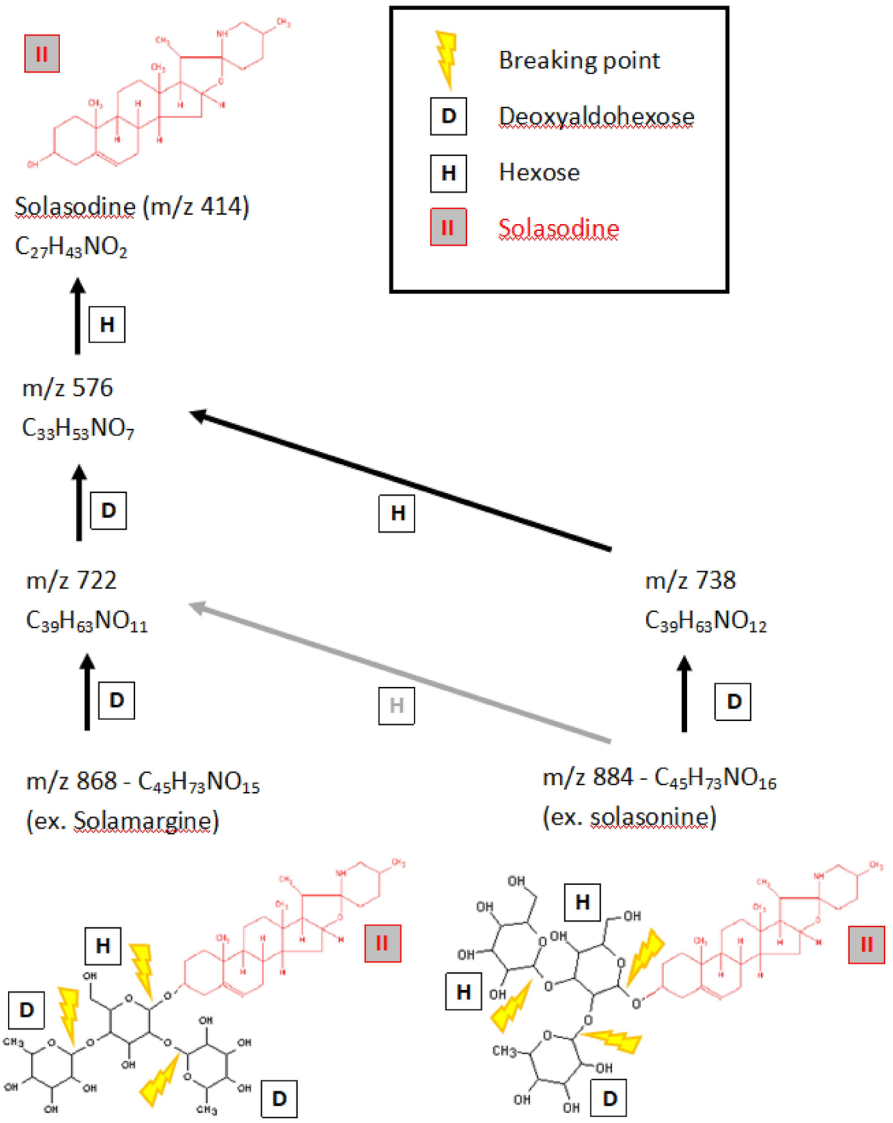

Fig. 2 Fragmentation patterns of tri-glycoalkaloids from *Solanum tuberosum* cv. Lady Rosetta with solasodine-like alkaloid precursor (II). The fragmentation pattern at *m/z* 868 corresponds to compounds B1, B2, and B3 (linear trisaccharide motifs), as well as B6 and B7 (Y-shaped trisaccharide motifs; α-solamargine, MSI level 1). The fragmentation pattern at *m/z* 884 corresponds to compounds C5 and C6 (Y-shaped trisaccharide motifs with a spectrum including *m/z* 722) and compounds C1 and C3 (linear trisaccharide motifs) (Table 3)

The relative abundance of these glycosylation motifs differed substantially between SGA families. Major SGAs, including α-chaconine, α-solanine and α-solamargine, were predominantly associated with branched trisaccharide structures, whereas several minor or low-abundance SGAs exhibited a higher proportion

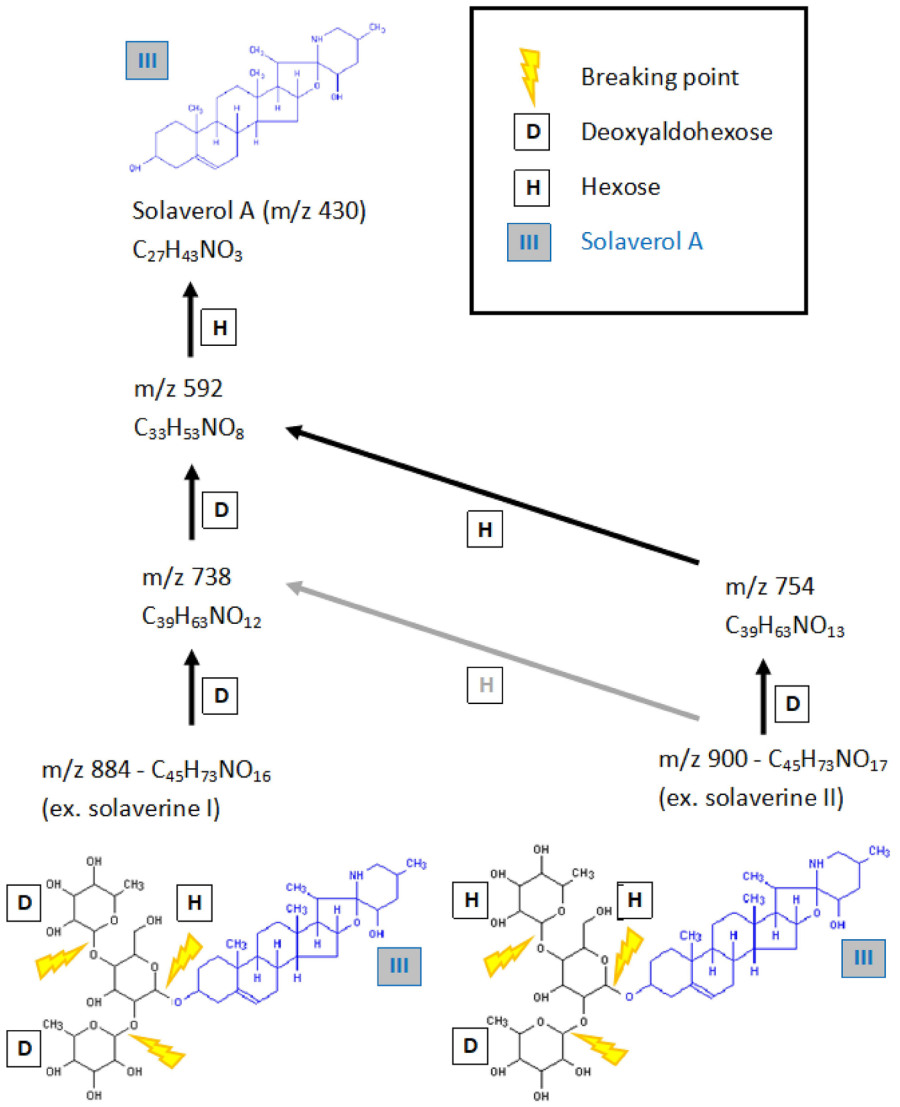

Fig. 3 Fragmentation patterns of tri-glycoalkaloids from *Solanum tuberosum* cv. Lady Rosetta with solaverol A-like alkaloid precursor (III). The fragmentation pattern at *m/z* 884 corresponds to compounds C2 (linear trisaccharide motifs), as well as C4 and C7 (Y-shaped trisaccharide motifs). The fragmentation pattern at *m/z* 900 corresponds to compounds D3 and D5 (Y-shaped trisaccharide motifs with a spectrum including *m/z* 722) and compounds D1 and D2 (linear trisaccharide motifs) (Table 3)

of linear glycosylation patterns. These observations may reflect that glycosylation contributes significantly to the structural diversification of potato SGAs in addition to aglycone oxidation.

Structural annotation confidence was assessed according to the Metabolomics Standards Initiative (MSI). α-Chaconine, α-solanine and α-solamargine were

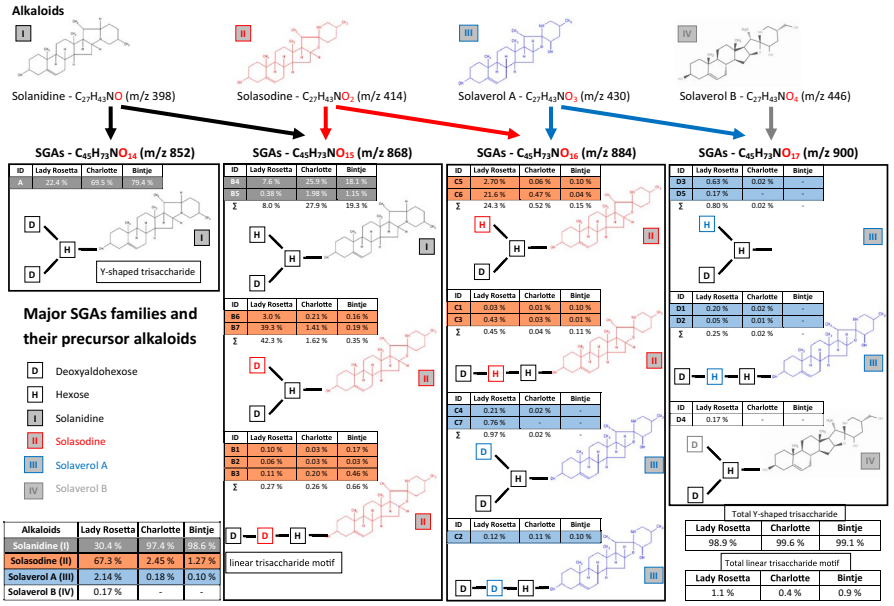

Alkaloids	Lady Rosetta	Charlotte	Bintje
Solanidine (I)	30.4 %	97.4 %	98.6 %
Solasodine (II)	67.3 %	2.45 %	1.27 %
Solaverol A (III)	2.14 %	0.18 %	0.10 %
Solaverol B (IV)	0.17 %	-	-

Total Y-shaped trisaccharide		
Lady Rosetta	Charlotte	Bintje
98.9 %	99.6 %	99.1 %

Total linear trisaccharide motif		
Lady Rosetta	Charlotte	Bintje
1.1 %	0.4 %	0.9 %

Fig. 4 Putative model of major SGA diversification with alkaloids, solanidine (I), solasodine (II), solaverol A (III) and solaverol B (IV) precursors of the SGAs and the different trisaccharide structures associated with. The schema included the relative signal contribution between each form SGAs (see ID in Table 3 and detailed structure information in Table 1) for the three cultivars of *Solanum tuberosum*, Lady Rosetta, Charlotte, and Bintje

confirmed at MSI level 1 using authentic analytical standards, whereas all other compounds were considered putatively annotated (MSI level 2 or 3) based on accurate mass, retention behaviour and diagnostic MS/MS fragmentation patterns (Salek et al. 2013; Rodríguez-Pérez et al. 2018). Although the observed fragmentation profiles were consistent with glycosylation pathways previously proposed for *Solanum* SGAs, the detailed trisaccharide organizations remain tentative for most compounds due to the absence of complementary structural validation by NMR.

Reconstruction of Major Biosynthetic Series

Integration of accurate mass measurements, chromatographic retention times and MS/MS fragmentation data enabled reconstruction of coherent biosynthetic series linking aglycone precursors to their corresponding glycosylated derivatives (Fig. 4; Tables 1 and 3).

The m/z 852 series was dominated by α-chaconine, which was consistently detected in all cultivars and represented one of the most abundant SGAs identified in potato leaves. Greater structural diversity was observed within the m/z 868 group, which included α-solanine, α-solamargine and several solasodine-derived isomers differing in glycosylation topology. Additional diversification occurred at m/z 884 and m/z 900, where multiple oxygenated SGAs associated with solaverol A and solaverol B aglycones were detected.

Table 1 For each retention time (RT), the m/z values of compounds involved in the major SGA proposed biosynthetic model inferred from LC–MS/MS data detected in leaf extracts of *Solanum tuberosum* cv. Lady Rosetta are reported, together with their fragmentation patterns. The presence of specific ions sharing the same RT and/or occurring within the same mass spectrum is indicated by a cross in the corresponding column. Only compounds yielding informative spectra with sufficient signal intensity were included in this table. In certain cases, compound identities were confirmed by comparison with analytical standards injected in solvent, showing identical retention times and mass spectra. Specifically, row A in the ID column corresponds to α-chaconine (m/z 852), row B4 to α-solanine (m/z 868), and row B7 to α-solamargine (m/z 868) confirmed at MSI level 1 using analytical standards (*) Fragment ions were considered after subtraction of 18 Da, corresponding to neutral loss of water. "???" indicates entries for which information was not available or was uncertain

		alkaloids precursors (m/z)				mono and di glyco-alkaloids (m/z)								SGAs (m/z)			
		398	414	430	446	560	576	592	608	706	722	738	754	852	868	884	900
ID	RT		(396)*	(394/412)*	(392/410/428)*		(558)*	(574)*	(590/572)*		(704)*	(720)*	(736)*	A	B (850)*	C	D
C1	9.6		x				x					x				x	
B1	10.0		x				x				x				x		
B2	11.1		x				x				x				x		
B3	11.8		x				x				x				x		
C2	11.8			x				???				x				x	
D1	12.1			x				x					x				x
C3	12.3		x				???					x				x	
D2	12.4			x				x					x				x
B4	12.5	x				x				x	x				x		
A	12.5	x				x				x				x			
C4	12.7			x				x				x				x	
B5	12.8	x				x				x	x				x		
D3	12.9			x				x				x	x				x
C5	13.1		x				x				x	x				x	
B6	13.2		x				x				x				x		
C6	13.5		x				x				x	x				x	
B7	13.7		x				x				x				x		
D4	14.1				x				x				x				x
D5	15.3			x				x				x	x				x
C7	15.3			x				x				x				x	

Dark grey indicates SGAs witch have solanidine (C27H43NO, m/z 398) like precursor

Blue indicates SGAs witch have solaverol A (C27H43NO3, m/z 430) like precursor

White or light grey indicates SGAs witch have solaverol B (C27H43NO4, m/z 446) like precursor

The same color code is used throughout the entire article

The reconstructed biosynthetic organization revealed pronounced cultivar-dependent differences. Lady Rosetta exhibited the most complex SGA network, combining solanidine-, solasodine- and solaverol-derived compounds across multiple mass series together with numerous isomeric forms. Charlotte displayed a more restricted profile dominated by solanidine-derived SGAs but retained a limited proportion of solasodine-related metabolites. In contrast, Bintje showed a simplified composition largely restricted to α-chaconine- and α-solanine-related compounds.

The coexistence of multiple aglycone backbones together with distinct glycosylation topologies highlights the extensive metabolic plasticity of potato SGA biosynthesis. The broader structural repertoire observed in Lady Rosetta further suggests enhanced diversification of late-stage oxidation and glycosylation processes relative to Charlotte and Bintje.

Cultivar-Dependent Variation in SGA Composition

Relative Distribution of Major SGA Families

Semi-quantitative comparison based on relative ion intensities revealed pronounced differences in SGA composition among the three potato cultivars (Fig. 7; Tables S1a and S1b). Although solanidine-derived SGAs were detected in all cultivars, their relative contribution to the total SGA pool varied substantially according to cultivar-specific metabolic profiles.

Bintje displayed the most restricted SGA composition and was strongly dominated by solanidine-derived compounds, which represented approximately 96% of relative ion abundance of detected aglycone precursors. Within this cultivar, α-chaconine-related metabolites accounted for the majority of the SGA signals, whereas oxygenated SGAs associated with solasodine or solaverol-type aglycones were detected only at trace levels. Charlotte exhibited an intermediate profile characterized by predominance of solanidine-derived SGAs together with limited accumulation of solasodine-related metabolites.

In contrast, Lady Rosetta showed a markedly broader structural diversity and accumulated high relative proportions of oxygenated SGAs. Solasodine-derived compounds represented approximately 65% of relative ion abundance of the total SGA pool in this cultivar, and additional solaverol-derived metabolites were consistently detected. Lady Rosetta also displayed the largest number of isomeric forms within individual mass series, indicating enhanced diversification through both aglycone oxidation and glycosylation processes.

These results demonstrate that SGA metabolism differs considerably among potato cultivars, particularly regarding the relative importance of oxidative modifications occurring upstream of glycosylation. The observed differences further suggest that the classical solanidine-dominated SGA profile does not fully represent the metabolic diversity present in potato leaves.

Biological Implications of SGA Diversification

The marked cultivar-dependent differences observed in SGA composition suggest that potato leaves possess distinct chemical defence profiles. Variations in both aglycone structure and glycosylation topology are likely to influence the physicochemical and biological properties of SGAs, including membrane interactions, toxicity and antimicrobial activity, as previously proposed for steroidal alkaloids in *Solanum* species.

The coexistence of multiple aglycone families together with structurally diverse trisaccharides may broaden the spectrum of biological activities associated with SGAs and contribute to differential responses toward herbivores and pathogens. In this context, the broader SGA diversity observed in Lady Rosetta may reflect enhanced metabolic plasticity and a more diversified defensive chemistry compared with the more restricted SGA composition detected in Bintje.

Although direct functional relationships were not investigated in the present study, previous studies have linked SGA composition to cultivar-specific resistance traits and ecological interactions. The present metabolomic data therefore support the hypothesis that qualitative SGA composition, rather than total glycoalkaloid abundance alone, may contribute to differences in potato defence potential.

More broadly, these findings highlight the importance of considering the full structural diversity of SGAs when evaluating potato specialized metabolism, as targeted analyses restricted to α-solanine and α-chaconine likely underestimate the biochemical complexity of potato leaf defense systems.

Low-Abundance SGA Pathways Reveal Additional Metabolic Complexity

Detection and Structural Characterization of Low-Abundance SGAs

In addition to the major SGA families, untargeted UHPLC–QTOF analysis consistently revealed several low-abundance steroidal glycoalkaloids across all investigated cultivars (Fig. 5; Tables 2 and 3). Although these metabolites represented only approximately 2.4–5.9% of relative ion abundance of the total SGA signal depending on the cultivar, they formed reproducible and structurally coherent metabolite series characterized by diagnostic aglycone-related fragment ions at m/z 396, 412 and 428.

Several observations support the interpretation of these compounds as genuine metabolites rather than analytical artefacts. These SGAs were reproducibly detected across biological replicates, displayed consistent chromatographic retention behaviour, and generated characteristic fragmentation patterns analogous to those observed for major SGAs. In particular, MS/MS spectra showed successive neutral losses corresponding to hexose and deoxyhexose residues, supporting the presence of tri-glycosylated structures closely related to the major SGA families.

The aglycone-related ions detected at m/z 396 and 412 were compatible with partially unsaturated or oxidized steroidal alkaloids structurally related to

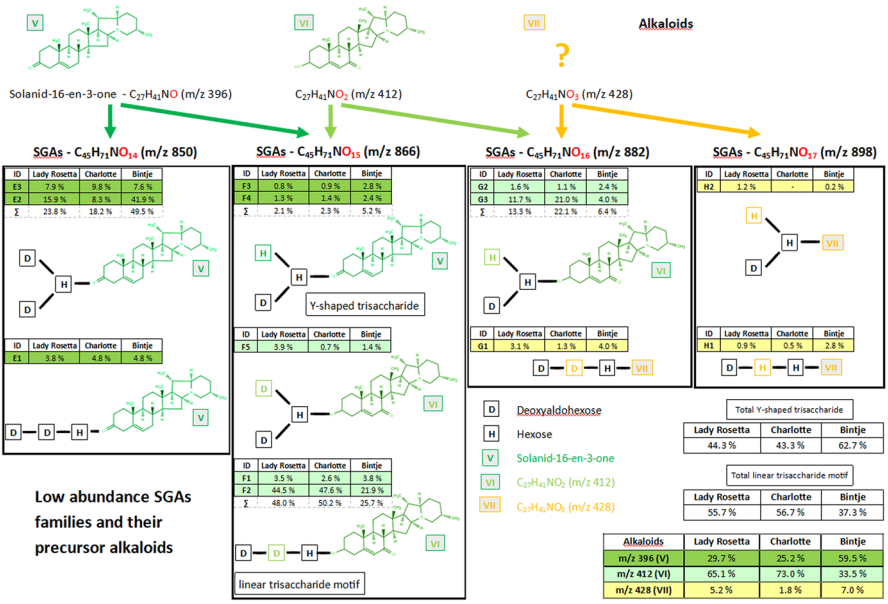

Fig. 5 Putative model of low abondance SGA diversification with partially unsaturated alkaloid backbones, m/z 396 (V), m/z 412 (VI) and m/z 428 (VII) precursors of the SGAs and the different trisaccharide structures associated with them. The schema included the relative signal contribution between each form SGAs (see ID in Table 3 and detailed structure information in Table 2) for the three cultivars of *Solanum tuberosum*, Lady Rosetta, Charlotte, and Bintje

solanid-16-en-type compounds previously reported in *Solanum* species. These metabolites differed from the canonical solanidine- and solasodine-derived SGAs by the loss of two hydrogen atoms, suggesting additional dehydrogenation reactions within the steroidal backbone. The recurrent detection of the m/z 428 ion was consistent with the presence of an additional oxygenated alkaloid precursor; however, no unambiguous structural assignment could be proposed based on currently available bibliographic and spectral data.

Although limited in-source fragmentation cannot be completely excluded as the origin of these compounds, their accurate masses, isotopic distributions, and chromatographic retention times are inconsistent with simple in-source fragmentation or dehydration products of the major SGAs. Collectively, these observations support the existence of additional low-flux biosynthetic branches contributing to the structural diversity of potato leaf SGAs.

Cultivar Distribution and Biological Significance of Low-Abundance SGAs

The relative distribution of low-abundance SGAs differed substantially among cultivars (Fig. 7; Tables S2a and S2b). In Bintje, these compounds were predominantly associated with the m/z 396 aglycone precursor, which accounted for approximately 60% of relative signal contribution of the low-abundance SGA pool. In contrast,

Table 2 For each retention time (RT), the m/z values of compounds involved in a low-abundance SGA proposed biosynthetic model inferred from LC–MS/MS data (not clearly identified) detected in leaf extracts of *Solanum tuberosum* cv. Lady Rosetta are reported, together with their fragmentation patterns. The presence of ions sharing the same RT and/or occurring within the same mass spectrum is indicated by a cross in the corresponding column. (*)Fragment ions were considered after subtraction of 18 Da, corresponding to neutral loss of water. "???" indicates entries for which information was not available or was uncertain

		alkaloids precursors (m/z)			mono and di glyco-alkaloids (m/z)							SGAs (m/z)			
ID	RT	396	412 (394)*	428 (410)*	558	574	590 (572)*	704 (686)*	720 (702)*	736 (706/718)*	752 (734)*	850 E	866 F	882 G	898 H
H1	9.4			x			x				x				x
G1	9.7			x			???			x				x	
G2	10.2		x			x			x	x				x	
F1	10.4		x			x			x				x		
G3	10.4		x			x			x	x				x	
F2	10.6		x			x			x				x		
E1	10.7	x			x			x				x			
E2	12.1	x			x			x				x			
F3	12.1	x			x			x	x				x		
E3	12.3	x			x			x				x			
F4	12.3	x			x			x	x				x		
H2	13.1			x			???				x				x
F5	13.3		x			x			x				x		

Dark green indicates SGAs witch have solanid-16-en-3-one (C27H41NO, m/z 396) like precursor

Light green indicates SGAs witch have oxygenated solanid-16-en-3-one (C27H41NO2, m/z 412) like precursor

Yellow indicates SGAs witch have dioxygenated solanid-16-en-3-one (C27H41NO3, m/z 412) like precursor

The same color code is used throughout the entire article

Table 3 List of compounds compatible with biosynthesis pathways of SGAs in *Solanum tuberosum* with in first column the ID corresponding to SGAs fragmentation spectrum and the alkaloids known (I to IV) like precursor in major proposed biosynthetic model inferred from LC–MS/MS data of SGAs and compounds potentially involved in low abundance proposed biosynthetic model inferred from LC–MS/MS data of SGAs (not identified). The isomeric forms are listed in parentheses in the ID column.

ID	Source	ID source	Monoisotopic mass	Average mass	Formula	ACD/IUPAC Name	Link
Alkaloids							
I	ChemSpider	59150	397.3345	397.636	C27H43NO	Solanidine	http://www.chemspider.com/Chemical-Structure.59150.html
II (a)	ChemSpider	391288	413.3294	413.636	C27H43NO2	Solasodine	http://www.chemspider.com/Chemical-Structure.391288.html
II (b)	ChemSpider	24534156	413.3294	413.636	C27H43NO2	Solasodine	http://www.chemspider.com/Chemical-Structure.24534156.html
III	ChemSpider	9114143	429.3243	429.635	C27H43NO3	Solaverol A	http://www.chemspider.com/Chemical-Structure.9114143.html
IV	Pubchem	274035867	-	445.635	C27H43NO4	Solaverol B	https://pubchem.ncbi.nlm.nih.gov/substance/274035867
V	ChemSpider	473852	395.318817	395.621	C27H41NO	Solanid-16-en-3-one	https://www.chemspider.com/Chemical-Structure.473852.html
SGAs							
A	ChemSpider	391274	851.5031	852.059	C45H73NO14	α-chaconine	http://www.chemspider.com/Chemical-Structure.391274.html
B5 (B4)	ChemSpider	7828094	867.4980	868.059	C45H73NO15	Solanine	http://www.chemspider.com/Chemical-Structure.7828094.html
B4 (B5)	ChemSpider	28033	867.4980	868.059	C45H73NO15	α-Solanine	http://www.chemspider.com/Chemical-Structure.28033.html
B7 (B6)	ChemSpider	66278	867.4980	868.059	C45H73NO15	α-Solamargine	http://www.chemspider.com/Chemical-Structure.66278.html
B1 (B2, B3)	ChemSpider	52563678	867.4980	868.059	C45H73NO15	Solamargine	http://www.chemspider.com/Chemical-Structure.52563678.html

Table 3 (continued)

C6 (C5)	ChemSpider	21468793	883.4929	884.058	C45H73NO16	Solasonine	http://www.chemspider.com/Chemical-Structure.21468793.html
C5 (C6)	ChemSpider	106525	883.4929	884.058	C45H73NO16	Solasonine	https://www.chemspider.com/Chemical-Structure.106525.html
C7 (C4)	ChemSpider	10270709	883.4929	884.058	C45H73NO16	Solaverine I	https://www.chemspider.com/Chemical-Structure.10270709.html
D3, D5 (D1, D2)	ChemSpider	10270710	899.4879	900.058	C45H73NO17	Solaverine II	https://www.chemspider.com/Chemical-Structure.10270710.html
D4	ChemSpider	10270711	899.4879	900.058	C45H73NO17	Solaverine III	https://www.chemspider.com/Chemical-Structure.10270711.html
F5	Pubchem	71725993	865.4824	866.0	C45H71NO15	-	https://pubchem.ncbi.nlm.nih.gov/compound/71725993
G2	Pubchem	162997758	881.4773	882.0	C45H71NO16	-	https://pubchem.ncbi.nlm.nih.gov/compound/162997758
G3	Pubchem	162997759	881.4773	882.0	C45H71NO16	-	https://pubchem.ncbi.nlm.nih.gov/compound/162997759

Lady Rosetta and Charlotte displayed more balanced distributions between m/z 396- and m/z 412-related metabolites together with occasional detection of m/z 428-derived species.

These cultivar-dependent differences suggest differential regulation of upstream aglycone modification steps involving dehydrogenation and/or oxidation reactions prior to glycosylation. Although the enzymatic basis of these transformations remains unresolved, the recurrent occurrence of these compounds across cultivars supports their integration within the broader SGA metabolic network rather than representing sporadic degradation products.

The biological significance of these low-abundance SGAs remains unclear. Nevertheless, their close structural relationship with the major SGA classes suggests that they may contribute to the overall chemical defence landscape of potato leaves either through direct biological activity or through modulation of SGA mixture composition. Minor structural variations within steroidal alkaloids have previously been associated with important changes in bioactivity (Paudel et al. 2017; Sonawane et al. 2018; Calf et al. 2019; Akiyama et al. 2021), indicating that even low-abundance compounds could influence ecological interactions (Lelario et al. 2019; Akiyama et al. 2021).

From an analytical perspective, the detection of these metabolites highlights the capacity of untargeted UHPLC–QTOF metabolomics to uncover previously overlooked layers of chemical diversity within potato SGAs. Analytical approaches focused exclusively on known glycoalkaloids such as α-solanine and α-chaconine would likely underestimate the complexity of potato steroidal alkaloid metabolism and overlook potentially relevant low-abundance biosynthetic pathways.

Proposed Model of SGA Glycosylation and Structural Diversification

Integration of accurate mass measurements, chromatographic retention behaviour, and MS/MS fragmentation patterns enabled the reconstruction of a coherent putative glycosylation framework underlying the structural diversification of potato steroidal glycoalkaloids (SGAs). The observed diversity of SGAs can be rationalized by sequential glycosylation of steroidal alkaloid aglycones through relatively conserved regioselective reactions, ultimately generating distinct trisaccharide architectures (Fig. 6).

Within this framework, glycosylation begins with the attachment of a hexose residue, typically glucose or galactose, to the aglycone hydroxyl group through an O-glycosidic linkage. The resulting monosaccharide conjugates can then undergo further glycosylation through either the addition of rhamnose to glucose-derived intermediates at C4 or the addition of a second glucose residue to galactose-derived intermediates at C3. Subsequent incorporation of a terminal rhamnose at C2 generates either branched Y-shaped or linear trisaccharide architectures, depending on whether the linkage involves the first or second sugar residue, respectively. The latter arrangement, although less frequently encountered, is exemplified by solamargine (e.g., ChemSpider ID 52563678; Table 3).

The fragmentation behaviour observed in MS/MS spectra provided strong support for this structural distinction. Branched trisaccharides containing two hexoses typically generated dual fragmentation pathways corresponding to alternative

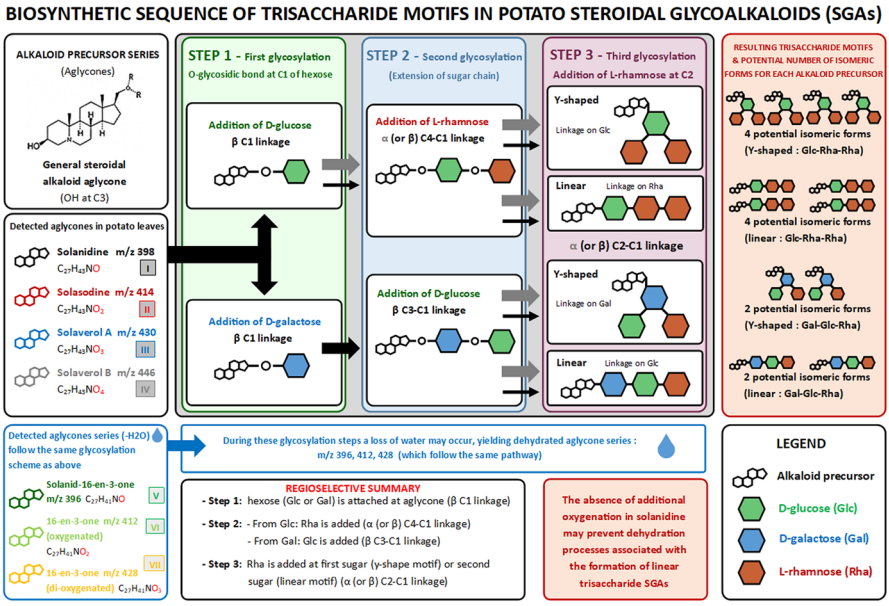

Fig. 6 Proposed model of trisaccharide diversification in potato steroidal glycoalkaloids (SGAs)

neutral sugar losses, whereas linear trisaccharides predominantly displayed sequential monosaccharide dissociation patterns. These observations were consistent across several aglycone series and were further supported by chromatographic retention behaviour, providing additional evidence for the proposed topological organization of the glycosidic chains.

Hexose residues are proposed to be β-linked, whereas rhamnose residues are generally α-linked, although β-rhamnose linkages may also occur (e.g., ChemSpider ID 28033, α-solanine, and ChemSpider ID 21468793, solasonine; Table 3). Variations in rhamnose stereochemistry may therefore contribute to the generation of multiple isomeric forms for a given trisaccharide topology. Additional observations consistent with this isomeric diversification hypothesis were provided by several highly accurate precursor ions (mass error < 1 ppm) that were excluded from structural annotation because no exploitable MS/MS spectra could be obtained (MSI level 4) and because each individual signal accounted for less than 0.01% of the total ion intensity. These unresolved features included two chromatographic peaks at m/z 868, five peaks at m/z 884, and one peak at m/z 900. Although their structural basis remains unknown, their chromatographic multiplicity is compatible with the occurrence of additional low-abundance isomeric forms predicted by the proposed glycosylation framework.

Reconstruction of the metabolite series further revealed a striking association between aglycone oxidation state and glycosylation topology. Linear trisaccharide motifs were exclusively associated with oxygenated aglycone series, including solasodine- and solaverol-derived metabolites, and systematically co-occurred with dehydrated intermediates. In contrast, solanidine-derived SGAs were restricted to branched trisaccharide architectures. Notably, no resolved isomeric forms were

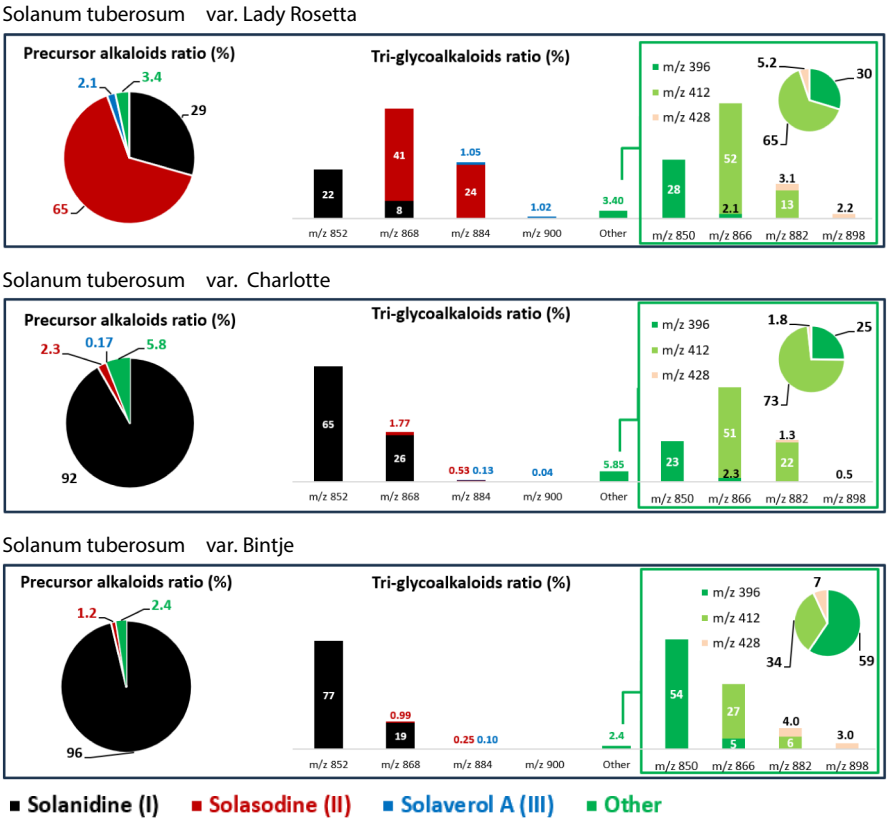

Fig. 7 Relative signal contribution (%) of potential free alkaloids based on SGAs measured and m/z of tri-glycoalkaloids with precursor origins for the three cultivars of *Solanum tuberosum*, Lady Rosetta, Charlotte, and Bintje. In green low-abundance SGAs with detailed ratio (%) (m/z of tri-glycoalkaloids and precursor alkaloids)

detected among monohexosylated solanidine intermediates, either because such species are absent or because they remain chromatographically indistinguishable under the analytical conditions employed. This apparent absence of detectable isomerism contrasts with the occurrence of two distinct isomeric forms among trisaccharide intermediates containing two hexose residues. The stage-dependent emergence of isomeric diversity suggests a specific organization of glycosylation reactions within the solanidine series. Collectively, these observations are consistent with a model in which dehydration events occurring during early glycosylation stages may contribute to the emergence of alternative, low-abundance glycosylation routes associated with the formation of linear SGAs.

Although these interpretations remain putative in the absence of direct enzymatic or NMR validation, the overall consistency observed between chromatographic behaviour, fragmentation pathways, predicted isomeric diversity, and cultivar-dependent metabolite distributions supports the biological plausibility of the proposed model. The

inferred sequence of glycosylation reactions was developed in the context of current knowledge regarding steroidal glycoalkaloid biosynthesis and the substrate selectivity of plant glycosyltransferases. Consequently, the proposed model should be viewed as a metabolomics-guided structural framework that is compatible with existing biosynthetic knowledge and provides a basis for future biochemical validation.

Conclusion

This study provides a comprehensive untargeted UHPLC–QTOF metabolomic characterization of steroidal glycoalkaloids (SGAs) in potato leaves and reveals extensive cultivar-dependent variation in both aglycone composition and glycosylation patterns. Beyond the classical solanidine-derived compounds α-solanine and α-chaconine, numerous additional SGAs associated with alternative and oxygenated aglycone backbones were detected, revealing a substantially broader structural diversity of potato leaf glycoalkaloids than previously recognized.

The metabolomic profiles obtained in this work highlight the remarkable plasticity of potato SGA metabolism and suggest the presence of multiple interconnected diversification processes contributing to glycoalkaloid structural complexity. In particular, the recurrent detection of oxygenated, partially unsaturated and low-abundance SGAs is consistent with the occurrence of additional low-flux metabolic routes that remain largely unexplored. The proposed glycosylation framework derived from MS/MS fragmentation patterns further provides a coherent structural interpretation linking aglycone oxidation state, trisaccharide topology and isomeric diversification.

Marked differences among cultivars further highlight substantial genotype-dependent variation in SGA composition and diversification patterns. Lady Rosetta displayed the broadest chemical repertoire, characterized by abundant solasodine- and solaverol-derived SGAs together with numerous isomeric forms, whereas Bintje exhibited a more restricted profile dominated by solanidine-derived compounds. Charlotte showed an intermediate metabolic organization between these two extremes. These cultivar-specific metabolite signatures further suggest differential organization of late-stage oxidation and glycosylation processes within potato specialized metabolism (Fig. 7).

More broadly, the present results demonstrate the value of untargeted UHPLC–QTOF metabolomics for resolving the complexity of steroidal alkaloid networks in potato. By enabling the simultaneous detection of both major and trace-level SGAs, this approach provides a substantially more comprehensive overview of potato chemical diversity than targeted analyses restricted to the principal glycoalkaloids.

Nevertheless, most detected SGAs remain putatively annotated based on metabolomic evidence and still require structural confirmation. Future studies combining targeted isolation, NMR spectroscopy, enzymatic characterization and functional bioassays will be necessary to validate the proposed structures and the glycosylation framework inferred from metabolomic data, clarify the origin of unresolved isomeric forms and determine the ecological and physiological significance of these newly detected metabolites. Collectively, these findings reveal a previously underappreciated level of structural diversity. within potato SGA metabolism and provide a framework for future biochemical and functional studies.

Supplementary Information The online version contains supplementary material available at https://doi.org/10.1007/s11540-026-10124-w.

Acknowledgements The authors would like to thank Vincent Cesar from Walloon Agricultural Research Centre for providing the potato cultivars used in this study.

Author Contribution Gilles Rousseau: conceptualization, methodology, formal analysis, software, supervision, visualization, writing—original draft, writing—review and editing.
Boris Krings: methodology, formal analysis.
Yordan Muhovski: methodology and writing review and editing.

Data Availability Raw and processed metabolomics data associated with this study will be made publicly available via XCMS Online upon publication.

Declarations

Competing interests The authors declare no competing interests.

References

Akiyama R, Watanabe B, Nakayasu M et al (2021) The biosynthetic pathway of potato solanidanes diverged from that of spirosolanes due to evolution of a dioxygenase. Nat Commun 12:1300. https://doi.org/10.1038/s41467-021-21546-0

Barre A, Bourne Y, Damme EJMV, Rougé P (2019) Overview of the structure–function relationships of mannose-specific lectins from plants, algae and fungi. International Journal of Molecular Sciences 20. https://doi.org/10.3390/ijms20020254

Calf OW, Huber H, Peters JL et al (2018) Glycoalkaloid composition explains variation in slug resistance in *Solanum dulcamara*. Oecologia 187:495–506. https://doi.org/10.1007/s00442-018-4064-z

Calf OW, Huber H, Peters JL et al (2019) Gastropods and insects prefer different *Solanum dulcamara* chemotypes. J Chem Ecol 45:146–161. https://doi.org/10.1007/s10886-018-0979-4

Delbrouck JA, Desgagné M, Comeau C, et al (2023) The therapeutic value of solanum steroidal (Glyco) alkaloids: a 10-year comprehensive review. Molecules 28. https://doi.org/10.3390/molecules28134957

EFSA Panel on Contaminants in the Food Chain (CONTAM), Schrenk D, Bignami M, et al (2020) Risk assessment of glycoalkaloids in feed and food, in particular in potatoes and potato-derived products. EFS2 18. https://doi.org/10.2903/j.efsa.2020.6222

Friedman M, McDonald GM, Filadelfi-Keszi M (1997) Potato glycoalkaloids: chemistry, analysis, safety, and plant physiology. Crit Rev Plant Sci 16:55–132. https://doi.org/10.1080/07352689709701946

Golan DE, Tashjian AH, Armstrong E et al (eds) (2005) Principles of pharmacology: the pathophysiologic basis of drug therapy. Lippincott Williams & Wilkins, Baltimore

Jared JJ, Murungi LK, Wesonga J, Torto B (2016) Steroidal glycoalkaloids: chemical defence of edible African nightshades against the tomato red spider mite, *Tetranychus evansi* (Acari: Tetranychidae). Pest Manag Sci 72:828–836. https://doi.org/10.1002/ps.4100

Lelario F, De Maria S, Rivelli AR et al (2019) A complete survey of glycoalkaloids using LC-FTICR-MS and IRMPD in a commercial variety and a local landrace of eggplant (*Solanum melongena* L.) and their anticholinesterase and antioxidant activities. Toxins (Basel) 11:230. https://doi.org/10.3390/toxins11040230

Martin P, Ahmed L, Lequart V, et al (2020) Natural and synthetic derivatives of the steroidal glycoalkaloids of solanum genus and biological activity. Natural product research 8:1–14. https://doi.org/10.35248/2329-6836.20.8.371

Massana-Codina J, Schnee S, Allard P-M, et al (2020) Insights on the structural and metabolic resistance of potato (Solanum tuberosum) cultivars to tuber black dot (Colletotrichum coccodes). Front Plant Sci 11. https://doi.org/10.3389/fpls.2020.01287

Middendorf PS, Jacobs-Reitsma WF, Zomer AL, et al (2022) Comparative analysis of L-fucose utilization and its impact on growth and survival of campylobacter isolates. Front Microbiol 13. https://doi.org/10.3389/fmicb.2022.872207

Nielsen SD, Schmidt JM, Kristiansen GH et al (2020) Liquid chromatography mass spectrometry quantification of α-solanine, α-chaconine, and solanidine in potato protein isolates. Foods 9:416. https://doi.org/10.3390/foods9040416

Paudel JR, Davidson C, Song J et al (2017) Pathogen and pest responses are altered due to RNAi-mediated knockdown of GLYCOALKALOID METABOLISM 4 in *Solanum tuberosum*. MPMI 30:876–885. https://doi.org/10.1094/MPMI-02-17-0033-R

Razgonova M, Kulikova V, Khodaeva V et al (2023) Simultaneous determination of steroidal alkaloids and polyphenol group from eight varieties of Siberian *Solanum tuberosum* L. through tandem mass spectrometry. Agriculture 13:758. https://doi.org/10.3390/agriculture13040758

Rodríguez-Pérez C, Gómez-Caravaca AM, Guerra-Hernández E et al (2018) Comprehensive metabolite profiling of *Solanum tuberosum* L. (potato) leaves by HPLC-ESI-QTOF-MS. Food Res Int 112:390–399. https://doi.org/10.1016/j.foodres.2018.06.060

Salek RM, Steinbeck C, Viant MR et al (2013) The role of reporting standards for metabolite annotation and identification in metabolomic studies. GigaSci 2:13. https://doi.org/10.1186/2047-217X-2-13

Scaglione F, Musazzi UM, Minghetti P (2021) Considerations on D-mannose mechanism of action and consequent classification of marketed healthcare products. Front Pharmacol 12. https://doi.org/10.3389/fphar.2021.636377

Sonawane PD, Heinig U, Panda S et al (2018) Short-chain dehydrogenase/reductase governs steroidal specialized metabolites structural diversity and toxicity in the genus *Solanum*. Proc Natl Acad Sci U S A 115:E5419–E5428. https://doi.org/10.1073/pnas.1804835115

Yamashita T, Fujimura N, Yahara S et al (1990) Structures of three new steroidal alkaloid glycosides, solaverines I, II and III from *Solanum toxicarium* and *S. verbascifolium*. Chem Pharm Bull 38:827–829

Authors and Affiliations

Gilles Rousseau[1] · Boris Krings[1] · Yordan Muhovski[2]

✉ Gilles Rousseau
g.rousseau@cra.wallonie.be

Boris Krings
b.krings@cra.wallonie.be

Yordan Muhovski
y.muhovski@cra.wallonie.be

[1] Protection, Control Products and Residues Unit, Knowledge and Valorization of Agricultural Products Department, Walloon Agricultural Research Centre, 11 Rue de Bordia, Gembloux 5030, Belgium

[2] Biological Engineering Unit, Life Sciences Department, Walloon Agricultural Research Centre, 234 Chaussée de Charleroi, Gembloux 5030, Belgium